Ductile Biodegradable Mg-Based Metallic Glasses with Excellent Biocompatibility

Hai-Jun Yu, Jun-Qiang Wang, Xue-Tao Shi, Dmitri V. Louzguine-Luzgin, Hong-Kai Wu,* and John H. Perepezko**

Magnesium-based metallic glasses (MMGs) show intriguing potentials for application as implantable biomaterials owing to their disordered atomic structure, good biodegradability, low elastic modulus, high strength, and large elasticity. However, despite of all these advantages, their brittleness is their Achilles' heel, which severely limits their application as biomedical materials. In the current study, a significantly improved ductility of MMGs under bending and tensile loading through minor alloying with rare-earth element ytterbium (Yb) at an atomic concentration of 2 and 4% is reported. The enhanced ductility is attributed to the increased density of shear bands close to fracture end and larger plastic zones on the fracture surface. In comparison with that of Yb-free control, in vitro cell culture study confirms an improved biocompatibility of MMGs alloyed with Yb as determined by MTT, live-dead, and cytoskeleton staining assays, respectively.

1. Introduction

The biodegradable implant materials are highly desired in repairing bone defects since they can degrade in vivo to avoid the chronic inflammation reaction and the secondary injury during removal of implant materials.[1–4] Among all the reported bone implant materials, Mg-based alloys have attracted a heightened attention owing to their biodegradability, and higher mechanical strength compared to their polymeric counterparts.[5–7] However, the biomedical application of crystalline Mg alloys was challenged with several drawbacks, including a higher elastic modulus than that of bone, higher corrosion rates compared to the growth rate of a bone, formation of hydrogen pockets near the implant site that may retard the healing process of the injury site, and local increase of alkalinity in the vicinity of Mg alloy-based implants.[8–11] To address all of these concerns of Mg-based crystalline alloys as biodegradable implant materials, MMGs with low elastic modulus, high strength and controllable corrosion rates have emerged as an attractive option.[12–15] The far-from-equilibrium state and the homogeneous atomic structure of metallic glasses (MGs) allow for dissolution of many different elements in large concentration not limited by the equilibrium phase diagrams. This characteristic has enabled researchers to tune the chemo-physical properties of metallic glasses in a wide range to meet the criteria for biomedical application.[11,15] However, the intrinsic brittleness is the common Achilles' heel of most of metallic glasses including MMGs, which seriously limits their application as structural or implant materials. Therefore, for the purposes of both laboratory fundamental research and clinical translational study, it is of great motivation to exploit the Mg-based metallic glasses with good ductility and excellent biocompatibility. Although extensive efforts had been devoted to exploiting ductile metallic glasses and investigating their plastic deformation mechanisms,[16–19] these efforts have unfortunately not yet yielded ductile MMG's.

Alloying with rare earth (RE) elements has been actively investigated to improve the mechanical and corrosion properties of Mg alloys.[20,21] The RE element Yb possesses similar chemo-physical properties as those of alkaline earth element calcium (Ca).[22] For example, both Yb and Ca can form divalent ions, have similar atomic size and elastic modulus. They are miscible with each other not only in liquid but also in crystalline solid state.[23] Importantly, it was reported that the corrosion resistance of Ca-based MGs was improved significantly by replacing Ca with Yb.[24]

Thus, in the current study, we focused efforts on improving the ductility of MgZnCa MGs by alloying with Yb. The mechanical properties of the as-prepared Yb-alloyed MMG were

Dr. H.-J. Yu, Dr. J.-Q. Wang, Dr. X.-T. Shi,
Prof. D. V. Louzguine-Luzgin, Prof. H.-K. Wu,
Prof. J. H. Perepezko
WPI Advanced Institute of Materials Research
Tohoku University
Sendai 980-8577, Japan
E-mail: jqwangexe@gmail.com; chhkwu@ust.hk; perepezk@engr.wisc.edu
Dr. H.-J. Yu
Center of Pharmaceutics
Shanghai Institute of Materia Medica
Chinese Academy of Sciences
Shanghai 201203, China
Prof. H.-K. Wu
Department of Chemistry
Hong Kong University of Science and Technology
Hong Kong SAR, China
Prof. J. H. Perepezko
Department of Materials Science and Engineering
University of Wisconsin-Madison
1509 University Avenue
Madison, WI 53706, USA

DOI: 10.1002/adfm.201203738

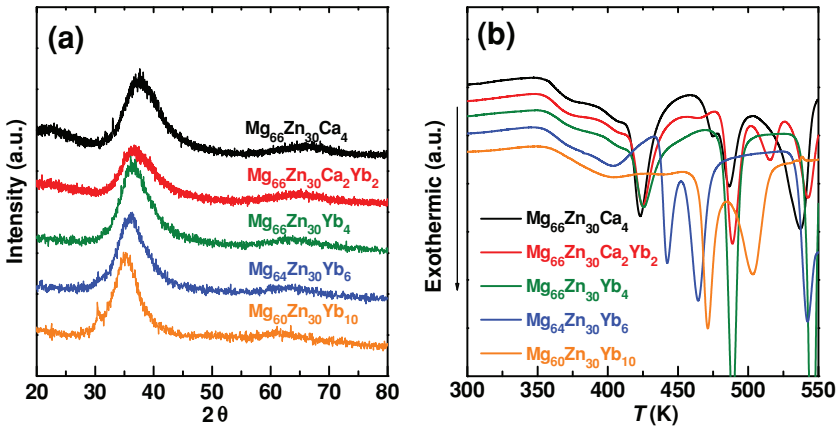

Figure 1. a) XRD patterns of Yb-alloyed MMG ribbons. The ribbons showed an amorphous atomic structure at low Yb-alloying percentages. When the Yb concentration was increased up to 10 at%, the glass forming ability of MMG became poor and the presence of crystalline phases was observed in the ribbon. b) DSC traces of the ribbons with different Yb concentrations. Exothermic crystallization events were clearly found which certifies the as-cast amorphous state of the ribbons at low Yb-alloying levels.

characterized by bending and tensile tests. The results demonstrated that the plasticity of MMGs was significantly improved by optimized Yb alloying. The in vitro biocompatibility of MMGs was also improved by Yb-alloying as confirmed by indirect cytotoxicity and direct cell adhesion, extension and proliferation assays.

2. Results

2.1. Microstructure and Thermal Properties

The atomic structure of Yb-alloyed MMGs was examined by X-ray diffraction (XRD) measurement. As shown in **Figure 1**a, no crystalline peaks were found in the XRD patterns of the MMG samples with Yb contents up to 6 at%, implying the amorphous structure of the as-prepared MMGs. On increasing Yb concentration to 10 at%, a weak crystalline peak was observed near 30°, which may be attributed to the presence of a metastable nanocrystalline phase. The formation of glassy atomic structure in the Yb-alloyed MMGs was further confirmed by the obvious exothermic crystallization peaks observed in differential scanning calorimetry (DSC) traces (Figure 1b). The absence of notable supercooled liquid region prior to crystallization suggested low thermal stability of the MMG samples.

2.2. Mechanical Properties

Good ductility of MMGs is crucial for their application as implantable stents. **Figure 2**a showed the tensile mechanical properties of Yb2 and Yb4 MMG samples measured at a strain rate of 0.0001 s^{-1}. The Young's elastic modulus and fracture strength of both MMG samples were close to each other, which were around 35 GPa and 500 MPa, respectively. In significant contrast, Yb0 control or other MMG samples with higher Yb contents (Yb6 and Yb10) were too brittle and broke at much lower stress (e.g., ≈30–100 MPa). The stress-strain curves of Yb2 and Yb4 samples start to deviate from the Hook linear elastic relation, and the acheived plastic strain was about 0.5%, suggesting their significantly improved plastic behavior compared to that of Yb0 control. The improved ductility of MMGs via Yb-alloying was also demonstrated by bending test as is shown in Figure 2b, where the ribbon (76 μm in thickness) of Yb2 sample with a mirror-like surface was not broken when bended even by about 180°. It is worth pointing out that MMGs with such a good plasticity has rarely been reported so far due to the difficulty to overcome the intrinsic brittleness of amorphous Mg alloys.[21]

The deformation mechanism of MGs under uniaxial stress has generated extensive attention of the scientific community. Although it is widely accepted that the initiation and propagation of shear bands account for the plastic deformation of the bulk samples at low temperatures,[25–28] it was recently shown that the shear band dominated heterogeneous plastic deformation may change to homogenous deformation when the sample size decreases down to sub-micrometer or nanometer scale.[19,29–31] These observations prompted us to examine the deformation behavior of the MMG samples at small size since a potential application of MMGs is vessel stents in sub-micrometer scale.[32,33] We took Yb2 MMG as an example to study the size-dependent plastic deformation behavior. As shown in **Figure 3**a, we found a small piece of sample near the fracture end of the ribbon sample. Along with the tensile deformation, dense shear bands with small shear offsets were formed to allow for the plastic deformation. The corresponding fracture surfaces

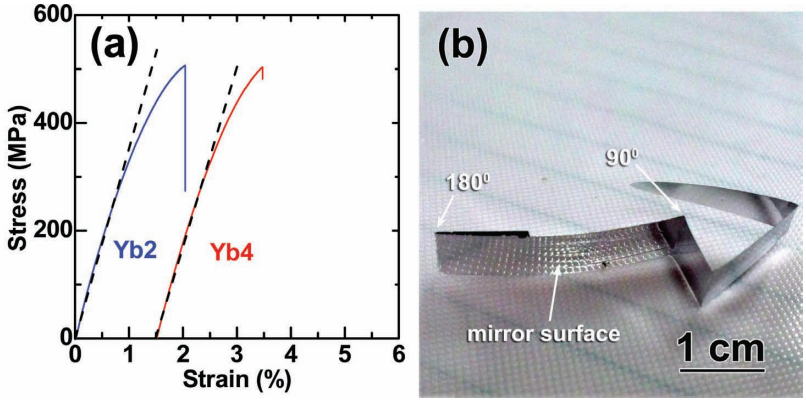

Figure 2. a) The plots of tensile stress versus strain curve at strain rate of 10^{-4} s^{-1} for the Yb2 and Yb4 ribbon samples. The plots indicate obvious yielding and plastic deformation behavior of Yb-alloyed MMG samples. b) The optical image of bent Yb2 MMG ribbon.

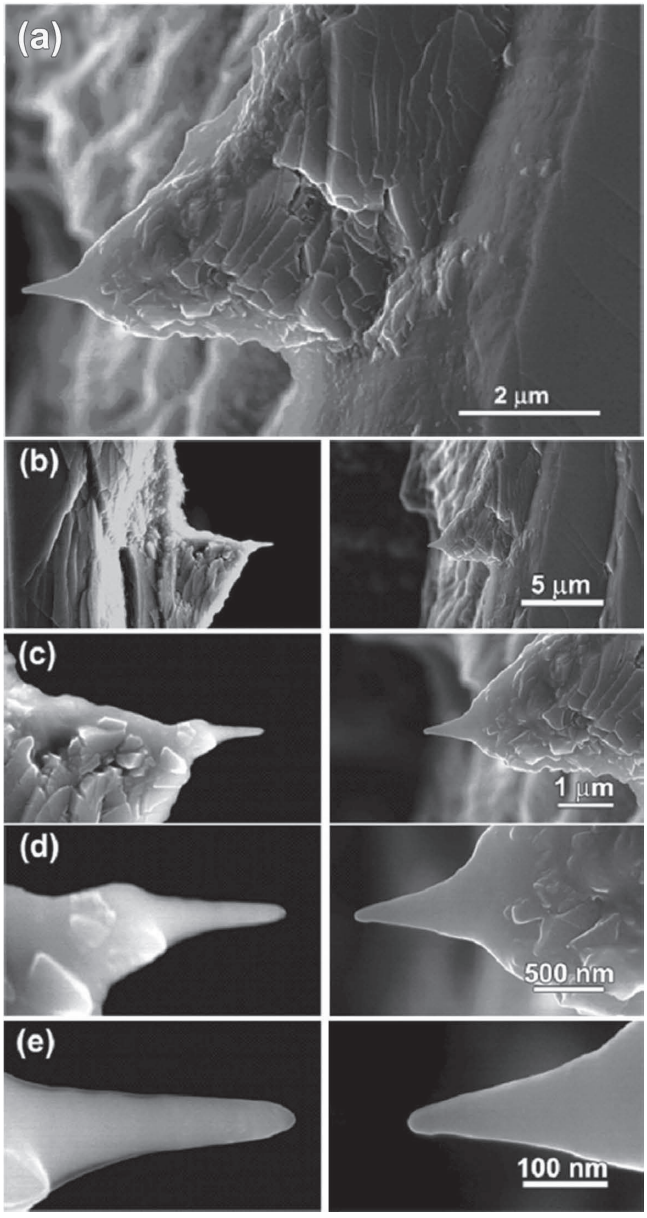

Figure 3. SEM images of the fracture end of Yb2 ribbon. a) The enlarged shear offsets and dense shear bands near the fracture end. b–e) show the two opposite fracture ends at graded magnifications. The transformation behavior from inhomogeneous (shear bands) to homogeneous deformation behavior can be observed clearly.

were shown in Figure 3b–e at gradient magnifications. Dense shear bands propagating in a direction having an angle of 45° to the tensile loading direction with a spacing distance of about ≈300–400 nm were observed near the fracture end. Interestingly, when the cross section size of the sample decreased to about ≈400–600 nm, close to the shear band spacing distance, the sample deformed homogeneously and no shear band was observed. The transformation of deformation behavior from heterogeneous to homogeneous is similar to the observations when pillar samples were compressed.[31] The absence of the shear bands in the plastic deformation at reduced section size may be attributed to the insufficiency of nucleation sites for shear bands[27,31] and the heat-assisted increase of surface diffusivity.[26]

2.3. Ion Concentration and pH of Immersion Solutions

The fast corrosion of alloy will release too much hydrogen gas and increase the pH of the body fluid for in vivo experiments which is bad for the recovery of body. To check the Yb-alloying effects on the corrosion resistance of MMGs, we performed the immersion experiments in simulated body fluid (SBF). The Mg ion release during SBF immersion was determined by ICP-MS measurement, and the results are shown in **Figure 4**a. In the initial stage of SBF immersion test (e.g., first 4 days), Yb0 sample showed the highest Mg^{2+} ion release rate. Mg^{2+} ion release from the MMGs samples became slow by alloying with Yb, and Yb10 sample displayed the lowest ion release rate. After 12 days of incubation, the Mg^{2+} ion concentration in the Yb0, Yb2 and Yb4 immersion solutions reached the highest level and then decreased gradually. This might be attributed to the growth of hydroxyapatite and precipitation of $Mg(OH)_2$ from the immersion solution at alkaline condition with concentrated Mg^{2+} ion, dominated by the dissolution-precipitation mechanism as proposed in the literature.[15,34]

Consistent with the pH increase trend, Figure 4b showed the pH change for the SBF immersed Yb-free and Yb-alloyed MMGs samples. In the first 8 days of immersion, the Yb0 control exhibited the fastest pH value increase compared to all other Yb-alloyed samples. The pH increase was reduced with increase in Yb content in the MMGs samples. After 12 days of immersion, the pH values of Yb0, Yb2 and Yb4 immersion samples became similar, while they were still higher than that of Yb6 and Yb10 ones. Among all MgZnCa(Yb) samples, Yb10 alloy caused the lowest pH increase at all testing durations.

2.4. Indirect Cytotoxicity Assay

The cytotoxicity of MMG samples was evaluated by MTT assay in vitro with extract concentration gradients. As shown in **Figure 5**a,b, at low Yb contents (e.g., Yb0, Yb2, Yb4 and Yb6), a negative correlation between cellular viability and extract concentration was found for both FB and OB cells. For example, at an extract concentration of 60%, all cells displayed good viabilities comparable to the untreated cell control. However, the cellular viabilities were reduced at increased extract concentrations. Importantly, the cells treated with complete Yb0 and Yb10 extracts showed the lowest (<10%) and the highest viability, respectively.

In order to investigate the influence of extract incubation on cellular morphology and cytoskeleton development, the cells were incubated with complete extract medium and examined by F-actin staining. As shown in Figure 5c,d, both FB and OB cells cultured in Yb0 extract displayed condensed cytoskeletal actin organization. When cultured in extracts of Yb-alloyed MMGs, the F-actin filaments of both types of cells became uniform. In the Yb10 sample, similar F-actin distribution and orientation was found as that of the cells cultured in the control medium, proved a positive correlation between Yb-alloying degrees and cellular biocompatibility of the MMG samples.

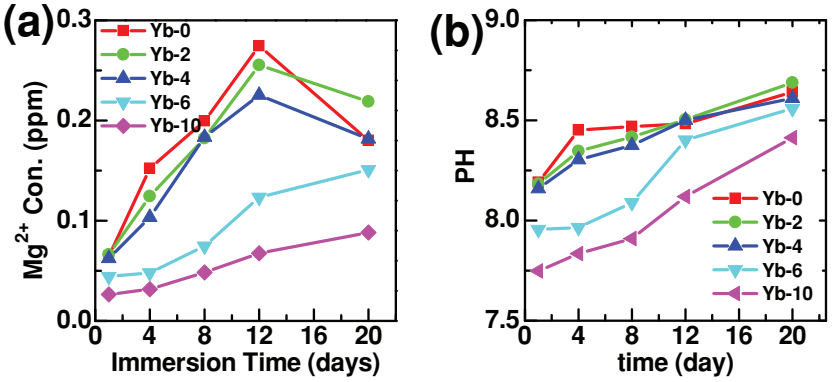

Figure 4. a) The concentration of Mg^{2+} ions released in the immersion solutions and b) the pH increase as functions of immersion time.

2.5. Direct Cell Adhesion and Proliferation

The biocompatibility of Yb-alloyed MMG samples was further evaluated by examining the adhesion, extension and proliferation of both FB and OB cells on MMG ribbons. As shown in **Figure 6**a,b, after 4 h incubation, both FB and OB cells efficiently attached on the surface of MMG ribbons independent of Yb-alloying concentrations. No obvious cellular extension was observed except that of FB cells growing on Yb6 ribbon. On extending the incubation time to 24 h, both FB and OB cells cultured on Yb0 surface retained condensed morphology. In obvious contrast, increased cell densities, well-developed cytoskeleton and largely-extended surface area were found for the cells growing on the Yb-alloyed MMG ribbons, implying the good biocompatibility.

In order to quantitatively evaluate the adhesion, extension and proliferation abilities of the cells growing on MMG ribbons, their relative growth rates and surface area were determined by normalizing with that of the control cells growing on the glass slide after 4 h incubation. Comparable amounts of FB or OB cells were found to attach onto MMG ribbons with different Yb-alloying concentrations after 4 h incubation (see Figure 6c). After a 24 h incubation, the numbers of FB cells increased over 3-fold as compared with those growing on the glass slide control, suggesting comparable proliferation ability of FB cells cultured on different MMG ribbons. In contrast, OB cells grew much slower on MMG samples than those cultured on the glass slide control (see Figure 6d), implying decreased cellular proliferation rates. After 24 h of incubation, as shown in Figure 6e,f, comparable surface area was found among both FB and OB cells cultured on a glass slide and MMG ribbons with high Yb contents (e.g., Yb4, Yb6 and Yb10). However, the surface area of the cells growing on the Yb0 ribbon was about 80% lower than that of the control cells. The inconsistence between the growth rate and extension degree of FB and OB cells cultured on Yb0 ribbon might be caused by its high cytotoxicity as proved by the MMT assay (see Figure 5a,b).

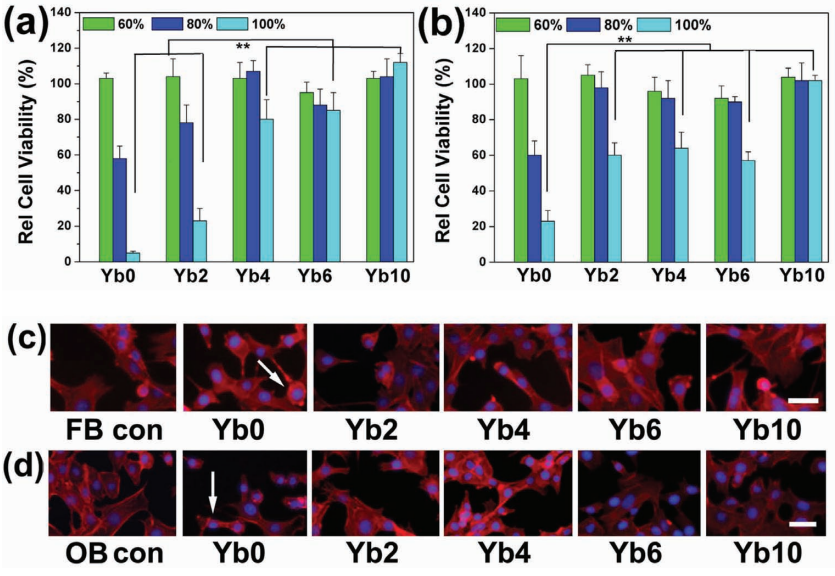

Figure 5. Relative viability of a) fibroblast (FB), and b) osteoblast (OB) cells cultured in MMG extract at different concentrations; Stained nuclei and F-actin patterns of c) FB and d) OB cells cultured in the complete extract medium, nuclear and F-actin were stained with DAPI and TMR-phalloidin, respectively (scale bar 50 μm, applied for all images).

3. Discussion

3.1. Micro-Mechanism of the Ductility

The emerging application of MMGs as biomedical materials is attracting increased attention owing to their unique characters. However, their brittleness is the major obstacles for clinical application of MMG based implant biomaterials. To address these challenges, an Yb-alloying strategy was employed to improve the ductility of MgZnCa MGs. For Yb2 and Yb4 MMG samples, the Young's elastic modulus of about 35 GPa is close to that of human bones (E = 3–27 GPa),[15] the fracture strength of about 500 MPa is ≈2–3 times higher than that of the commercial Mg-based alloys,[3,35] and 5 times higher that of biodegradable HA/PLLA hybrid scaffold.[36] The as-prepared Yb2 and Yb4 MMG can deform plastically as demonstrated by bending and tensile tests.

Shear bands (SBs) in MGs are supposed to play a similar role to dislocations in crystals, both of which are responsible for the plastic deformations since extensive SBs are usually found in ductile MGs after plastic deformation.[16] To exploit the mechanism for plastic deformation of Yb-alloyed MMGs, the shear bands formed during tensile testing were investigated by SEM examination. **Figure 7**a–e shows the side-view near the fracture surface of the ribbons with Yb concentrations of 0, 2, 4, 6, and 10 at%, respectively. Multiply shear bands leading to shear offsets on the surface

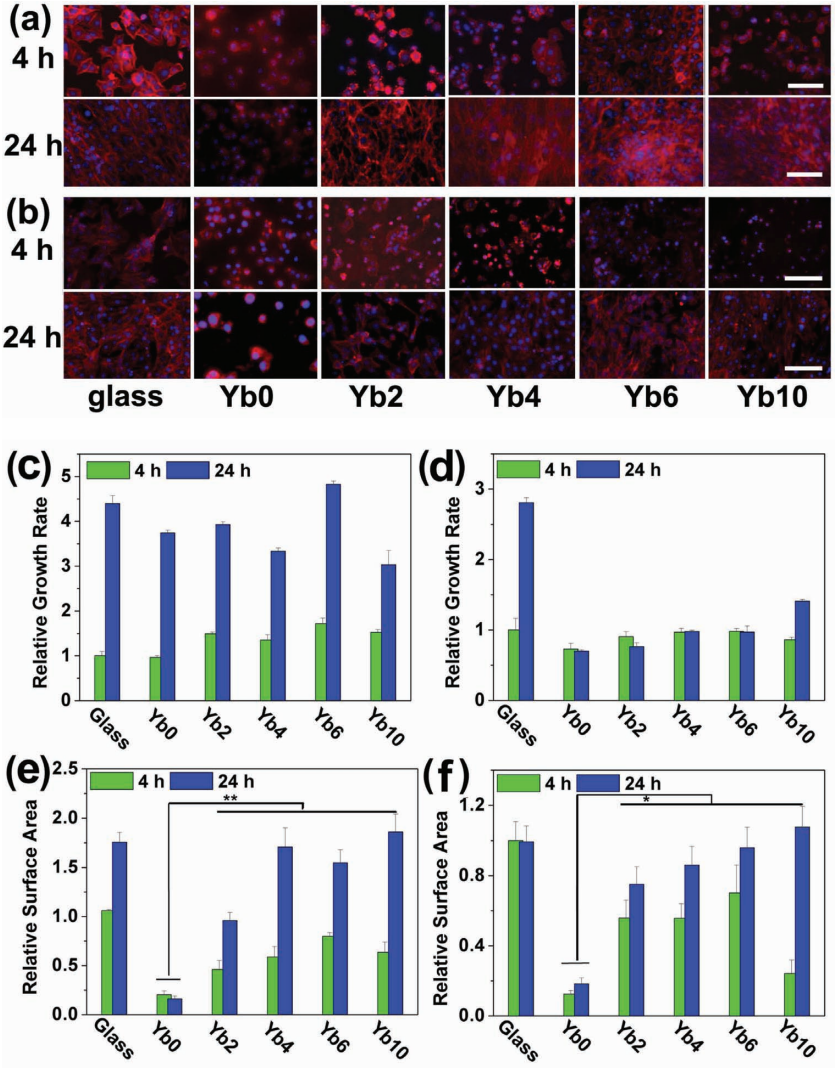

Figure 6. Adhesion and proliferation behaviors of a) FB and b) OB cells as examined by nuclei and F-actin staining assay. The cells were cultured on MMG sheets with different Yb-alloying concentrations and stained with DPAI and TMR-phalloidin 4 h and 24 h later after cell seeding, respectively (scale bar 50 μm, applied for all images). The relative growth rate and relative surface areas of c,e) FB and d,f) OB cells cultured on Yb-alloyed MMG sheets. The cells numbers were counted 4 h and 24 h later after cell seeding, respectively. The corresponding cellular surface areas were measured with image-J software. The cell numbers and cell surface areas were normalized with that of cell controls cultured on a glass cover slide after 4 h incubation.

were clearly observed. In comparison with other MMG samples, the Yb2 and Yb4 samples showed higher density of SBs near the fracture surface. This is consistent with the results of mechanical tests.

On the other hand, as shown experimentally, the size of dimples on the fracture surface can be used as another parameter to evaluate the plasticity or fracture toughness of metallic materials.[28,37] The morphology of the fracture surface of these alloys was examined using high-resolution SEM, and the results are shown in **Figure 8**a–e. The dimple morphology for the present Yb-alloyed MMG samples is similar to that of other MGs reported earlier.[28,38,39] The dimple sizes were plotted against Yb concentration as shown in Figure 8f. When 2 or 4 at% of Yb was added, the size of dimples on the fracture surface was much larger than that for other MMGs. Given the positive correlation between dimple size and high toughness or plasticity,[26] a high toughness and good plasticity is expected for the Yb2 and Yb4 samples. This is consistent with the results from the mechanical testing.

The characterization length of the plastic zone size can be expressed as $d \propto \frac{\chi}{G}$, with χ is the surface tension and G is shear modulus.[[40] Then, the increased plastic zone size may be attributed to the low shear modulus and high surface tension. On the other hand, it is supposed that shear bands are developed from the activation and percolation of shear transformation zones, whose activation energy is proportional to the shear modulus.[41] Thus, the lower shear modulus gives lower energy barrier for shear transformation zones which would benefit the formation of more shear bands. So, the enhanced ductility could be attributed to the decrease of shear modulus after the alloying of Yb. Our previous work has shown that the minor alloying of Yb in MgZnCa metallic glass system can reduce the atomic packing density, which probably induce a lower elastic modulus, then benefit the plastic deformability.[24]

3.2. Mechanism for Improved Biocompatibility Via Alloying with Yb

Given the suppressed pH increase and Mg^{2+} ion release of MgZnYb MMGs as compared with Yb free one, we concluded that Yb-alloying improved the corrosion resistance of MgZn MGs. Our observation was also supported by the literature reports that minor RE alloying could improve the mechanical properties and corrosion resistance of MGs.[42,43] On the other hand, the reduced corrosion rate by Yb-alloying will also suppress the release of harmful hydrogen gas produced by the corrosion of MMGs, which is good in vivo for the healing process of the injury site.[11]

As demonstrated in the indirect cytotoxicity, direct cell adhesion and proliferation studies, Yb-alloying is a feasible strategy to improve the biocompatibility of MMGs. To exploit the mechanism of MMG extract caused cell death, both FB and OB cells were incubated with complete MMG extract and examined by live-dead assay. The cytosol and nuclei of untreated control cells displayed green and blue color as stained with Calcein-AM and Hoechst 33342, respectively, suggesting good cytoplasm membrane integrity (see the top panel or the bottom right images in **Figure 9**a,b. In obvious contrast, when incubated with Yb0 extract, both of FB and OB cells shrank and the dead cells

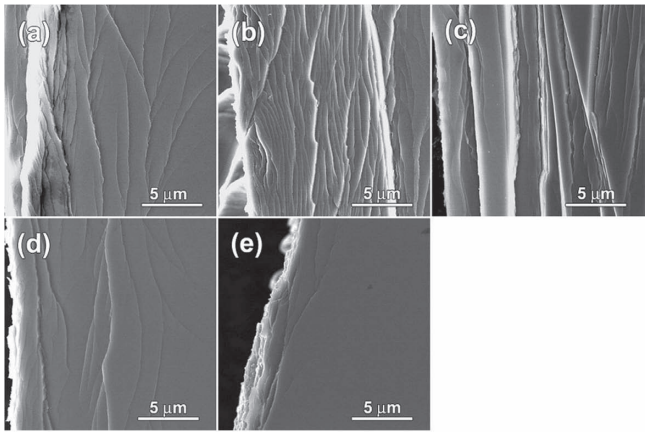

Figure 7. Typical SEM images of the shear band morphology near the fracture surface of Yb-alloyed MMG ribbons: a) Yb0, b) Yb2, c) Yb4, d) Yb6, and e) Yb10. Dense shear bands were observed in Yb2 and Yb4 MMG samples implying their good plasticity.

were stained as red. As treated with MMG extracts with 4 at% or higher Yb concentrations, the ratios of red cells in total cell populations decreased obviously as examined by fluorescence microscopic observation due to improved biocompatibility of MgZnYb MMGs, in consistent with the results of MTT assay. No notable difference was found among Hoechst stained nucleus of live and dead cells (shown in left-bottom insert in Figure 9a,b, indicating no DNA damage during cell death. Thus, the dead cells may undergo necrosis pathway, which might be attributed to the high Mg ion concentration and high pH value of the extract induced cell membrane damage. It was reported that increase of Ca content would cause fast corrosion of MgCa alloys.[3] In the case of Yb4 sample, all calcium element was completely substituted with 4 at% Yb alloying, thus improving the corrosion resistance of MgZn alloys.

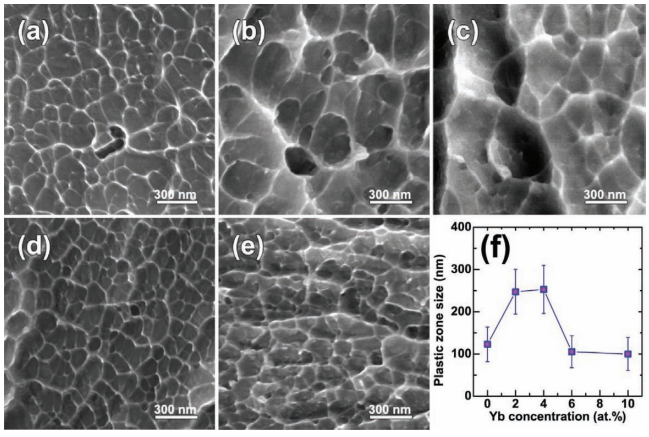

Figure 8. SEM images of the fracture surface of the samples with different Yb concentrations, a) 0 at%, b) 2 at%, c) 4 at%, d) 6 at%, and e) 10 at%, respectively. f) Plot of plastic zone size as a function of Yb-alloying concentration; the plastic zone size was averaged from 50 measurements for each sample. Bigger plastic zones were found in Yb2 and Yb4 MMG samples than other MMGs, suggesting their good plastic property.

Although only minor difference in pH increase and Mg^{2+} ion release was found between Yb4 and Yb0 control, the biocompatibility of Yb4 MMG was significantly improved, which was assumed to be attributed to the reduced alkalization near the surface of MgZnYb alloys.

4. Conclusion

In this work, we demonstrated that Yb alloying could significantly improve the ductility and biocompatibility of MMGs, both of which are essential for the application of MMGs as implants. It was found that:

(1) MgZnCa glassy alloy can be made ductile via Yb-alloying as confirmed by mechanical tests and the presence of the extensive shear bands near the fracture end and large plastic zones on the fracture surface in Yb2 and Yb4 MMGs. The increased plasticity may derive from the decrease of the shear modulus after Yb-alloying.
(2) The plastic deformation regime changes from shear band-dominated heterogeneous behavior to homogeneous behavior when the sample size decreases to about 500 nm.
(3) Cell culture study in vitro showed that alloying with minor Yb can reduce the indirect and direct cytotoxicity of MMGs at Yb concentration of 4 at% or higher, which was proposed to be attributed to the reduced alkalization near the surface of MgZnYb alloys.
(4) Taking into consideration of all the results of mechanical test and cellular biocompatibility assays plus minimal cytotoxicity of Yb metal, we conclude that Yb4 ($Mg_{66}Zn_{30}Yb_4$) alloy is the most potent candidate for use as implant biomaterial.

It is worth to note that the Mg-based metallic glasses have ever been thought to be among the most brittle glassy alloys. However, our findings show that they can be ductile by adjusting the compositions. These results may provide new opportunity to promote both the fundamental research and their applications.

5. Experimental Section

Materials Fabrication and Characterization: The pure metals of Mg, Zn, Ca, and Yb (purity > 99.9 wt%) in nominal compositions (at%) of $Mg_{66}Zn_{30}Ca_4$ (Yb0), $Mg_{66}Zn_{30}Ca_2Yb_2$ (Yb2) $Mg_{66}Zn_{30}Yb_4$ (Yb4), $Mg_{64}Zn_{30}Yb_6$ (Yb6) and $Mg_{60}Zn_{30}Yb_{10}$ (Yb10) were melted together according to the nominal composition ratios in a BN crucible using an induction melting method. The master alloys were then remelted in a quartz tube using induction melting and subsequently injected on a copper roller to spin into ribbons with thickness of between 40 and 100 μm. The furnace chambers used here were initially pumped to a high vacuum of <0.003 Pa and then backfilled by high purity Ar gas to protect from oxydation. The atomic structure of the as-prepared ribbons was characterized by X-ray diffraction (XRD, Bruker D8 Advance diffractometer equipped with a Cu-$K\alpha$ radiation). The glass transition and crystallization behaviors of the as-prepared MMGs were studied by differential scanning calorimetry measurement (DSC, Perkin-Elmer 8500 machine) at a heating rate of 40 K/min.

Mechanical Tests: The deformation plasticity of the ribbons was evaluated by bending and tensile test methods. The ribbon samples in suitable size (e.g., 40 μm in thickness, 3 mm in width and 30 mm in length) were used for tensile testing at a constant strain rate of

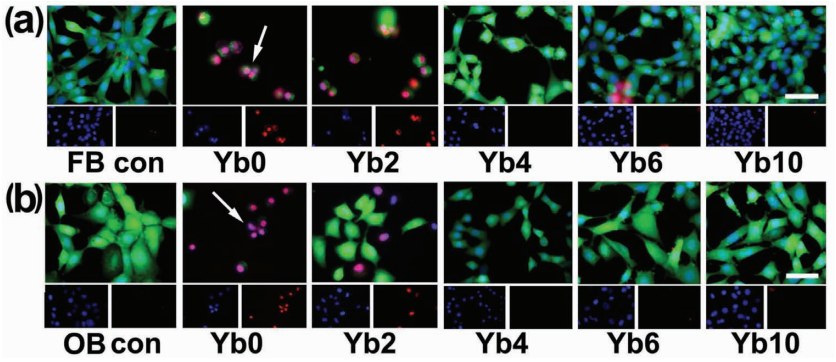

Figure 9. Live-dead-apoptosis assay of a) FB and b) OB cells incubated in complete medium extract, the top panel shows the overlapped images of cells stained by Calcein-AM (green), Hoechst 33342 (blue, also in left-down inserted images) and EthD-1, respectively, the bottom panel shows the separated fluorescent images of cells stained with Hoechst 33342 and EthD-1, respectively (scale bar 50 μm, applied for all images).

10^{-4} s^{-1} at room temperature. To make sure the reliability of the mechanical tests, we have repeated the measurements and found that the result can be reproductive. The test of other metalic glassed with a different composition, e.g., $Cu_{47.5}Zr_{47.5}Al_5$, did not show the plasticity. So, we can say that the tensile experiment is reliable without any experiment artifacts. These data can be found in the Figure S1 and S2 in the Supporting Information. The morphology of shear bands and fracture surface were examined using high-resolution scanning electron microscope (SEM, Hitachi S-4800 Scanning Electron Microscope).

Immersion Test: The immersion test was carried out at different time points to monitor the degradation and magnesium ion release of the Yb-alloyed MMGs. The samples were individually immersed into sealable capsules in simulated body fluid (SBF) containing 10 mg·mL^{-1} of MMGs. The capsules were then incubated at 37 °C for a total of 20 days. The release of magnesium ions from the samples was measured at 5 different time points (1, 4, 8, 12, and 20 days) using inductively-coupled plasma mass spectrometry (ICP-MS, AXIS-ultra, Shimadzu Kratos). In addition, the pH values were also measured for each of the samples at each time point. The SBF solution was prepared according to a published recipe (NaCl 8.035 g, $NaHCO_3$ 0.355 g, KCl 0.225 g, $K_2HPO_4{\cdot}3H_2O$ 0.231 g, $MgCl_2{\cdot}6H_2O$ 0.311 g, $CaCl_2$ 0.292 g, Na_2SO4 0.072 g, $(HOCH2)_3CNH_2$ 6.118 g for 1000 mL solution).[44]

Cell Culture: Murine fibroblast (FB) NH3T3 and murine osteoblast (OB) cells were obtained from ATCC and used for in vitro cell culture study. The FB and OB cells were cultured in Dulbecco's Modified Eagle's medium (DMEM) and Minimum Essential medium (MEM) alpha medium, respectively. Both kinds of media contain 10% of fetal bovine serum (FBS), 100 U·mL^{-1} penicillin and 100 mg·mL^{-1} streptomycin. The cells were cultured at 37 °C incubator with humidified atmosphere and 5% CO_2 concentration.

Indirect Cytotoxicity Test: The MMGs samples were extracted in serum-free DMEM medium at a concentration of 10 mg/mL and incubated at 37 °C for 8 days. The supernatant fluid was withdrawn and centrifuged to prepare the extraction medium, then stored in a 4 °C refrigerator before use for cytotoxicity testing. The untreated medium was used as a negative control. For cytotoxicity assay, FB or OB cells were incubated in 96-well tissue culture plates at a density of 5×10^3 cells per well with addition of 100 μL of cell culture medium. The cells were incubated for 24 h to allow for attachment. The medium was then replaced with 100 μL of fresh cell culture medium containing different percentages of extracts (60%, 80% and 100%) with 10% FBS supplementary. After 24 h of incubation, the metabolic activity of the extracts treated cells was determined by MTT assay and the results were expressed as relative cell viability normalized with that of the untreated cell control.

Live-Dead-Apoptosis Assay: FB or OB cells were incubated in 96-well cell culture plates at a density of 5×10^3 cells per well in 100 μL of cell culture medium. The cells were pre-incubated for 24 h to allow for attachment. The medium was then replaced with 100 μl of complete extraction medium containing 10% of FBS. After 24 h of incubation, the cells were rinsed with PBS and stained with Calcein-AM (Invitrogen), Ethdium homodimer-1 (EthD-1, Invitrogen) and Hoechst 33342 (Invitrogen) for live, dead and apoptosis assay, respectively. The stained cells were examined using inverted fluorescence microscopy equipped with DAPI, GFP and Cy3 filter sets (Axio Observer Z1, Carl Zeiss, Japan). The live-dead-apoptosis assay solution was prepared by diluting Calcein (AM) (4.0 M solution in DMSO), ethidium homodimer-1 (EthD-1, 2.0 M solution in DMSO) and Hoechst 33342 (10 mg/mL solution in PBS) stock solutions in PBS at final concentrations of 2.0 μM, 2.0 μM and 2.5 μg/mL, respectively. Calcein-AM can penetrate into both live and dead cells, but can only be activated in live cells to produce green fluorescence. Ethdium homodimer-1 (EthD-1), a red-fluorescence dye, is only permanent to dead cells. Hoechst 33342, a blue-fluorescence dye (excitation/emission maxima ≈350/461 nm, when bound to DNA), stains the condensed chromatin in apoptotic cells more brightly than the chromatin in normal cells. Thus, the staining pattern produced from the simultaneous use of these three different dyes makes it possible to distinguish normal, apoptotic, and necrotic cells by fluorescence microscopy exanimation.

Cytoskeleton Examination: The cells were firstly incubated with medium extract for 24 h, and then the cellular cytoskeleton structure was examined by nuclear/F-actin staining assay. In brief, the cells were fixed with 4% paraformaldehyde (Sigma) for 15 min and subsequently permeabilized with 0.1% Triton X-100 (Sigma) for 5 min. After gently rinsing with PBS for three times, the cells were stained with tetramethylrhodamine (TMR)–phalloidin (Invitrogen) for F-actin and 4,6-diamino-2-phenyl-indole (DAPI) (Invitrogen) for nuclei, respectively. The cytoskeleton structure of the stained cells was then visualized by fluorescence microscopy.

Cell Adhesion, Extension and Proliferation: To evaluate the adhesion, extension and proliferation of FB and OB cells on Yb-alloyed MMGs, all MMG samples with different Yb-alloying degrees were fixed on the same glass cover slide (24 mm × 24 mm), sterilized by overnight immersion in 75 vol% ethanol and lastly 30 min UV radiation (253.5 nm). The sterilized MMG samples were put into 60 mm tissue culture dish with addition of 10 mL FB or OB cell suspension containing 5×10^6 cells. After 4 h, 24 h or 72 h incubation, the cells were fixed with paraformaldehyde (Sigma) and then exposed for F-actin and nuclei staining, respectively. The cell number on each MMG samples was determined by counting the DAPI stained nuclei in images taken with a 10× lens. The cell surface area was measured with ImageJ software (NIH, USA), and the results were averaged from the surface area of more than 50 cells. The cell growth and proliferation rate were expressed as relative growth rate and relative surface area after normalized with that of the control cells growing on the glass cover slide after 4 h incubation.

Statistical Analysis: Data were presented as the mean ±SD of three replicates. The statistical significance was determined by using the analysis of variance (ANOVA). *: $p < 0.05$, **: $p < 0.01$, P value <0.05 was considered significant.

Supporting Information

Supporting Information is available from the Wiley Online Library or from the author.

Acknowledgements

H.J.Y. and J.Q.W. contribututed equally to this work. This work was supported by the Fusion Research Fund sponsored by World Premier International Research Center Initiative-Advanced Institute of Materials Research (WPI-AIMR), MEXT, Japan.

Received: December 17, 2012
Published online: April 26, 2013

[1] S. J. Hollister, *Nat. Mater.* **2005**, *4*, 518.
[2] M. P. Staiger, A. M. Pietak, J. Huadmai, G. Dias, *Biomaterials* **2006**, *27*, 1728.
[3] Z. J. Li, X. N. Gu, S. Q. Lou, Y. F. Zheng, *Biomaterials* **2008**, *29*, 1329.
[4] F. Witte, H. Ulrich, M. Rudert, E. Willbold, *J. Biomed. Mater. Res. A* **2007**, *81A*, 748.
[5] T. Kraus, S. F. Fischerauer, A. C. Hanzi, P. J. Uggowitzer, J. F. Loffler, A. M. Weinberg, *Acta Biomater.* **2012**, *8*, 1230.
[6] F. Witte, *Acta Biomater.* **2010**, *6*, 1680.
[7] M. C. Serrano, E. J. Chung, G. A. Ameer, *Adv. Funct. Mater.* **2010**, *20*, 192.
[8] C. Y. Zhang, R. C. Zeng, C. L. Liu, J. C. Gao, *Surf. Coat. Technol.* **2010**, *204*, 3636.
[9] M. D. Pereda, C. Alonso, L. Burgos-Asperilla, J. A. del Valle, O. A. Ruano, P. Perez, M. A. F. L. de Mele, *Acta Biomater.* **2010**, *6*, 1772.
[10] J. E. Gray-Munro, C. Seguin, M. Strong, *J. Biomed. Mater. Res. A* **2009**, *91A*, 221.
[11] B. Zberg, P. J. Uggowitzer, J. F. Loffler, *Nat. Mater.* **2009**, *8*, 887.
[12] E. Ma, J. Xu, *Nat. Mater.* **2009**, *8*, 855.
[13] J. Schroers, G. Kumar, T. M. Hodges, S. Chan, T. R. Kyriakides, *JOM* **2009**, *61*, 21.
[14] G. Y. Yuan, C. L. Qin, A. Inoue, *J. Mater. Res.* **2005**, *20*, 394.
[15] X. N. Gu, Y. F. Zheng, S. P. Zhong, T. F. Xi, J. Q. Wang, W. H. Wang, *Biomaterials* **2010**, *31*, 1093.
[16] Y. H. Liu, G. Wang, R. J. Wang, D. Q. Zhao, M. X. Pan, W. H. Wang, *Science* **2007**, *315*, 1385.
[17] J. C. Ye, J. Lu, C. T. Liu, Q. Wang, Y. Yang, *Nat. Mater.* **2010**, *9*, 619.
[18] Y. Wu, Y. H. Xiao, G. L. Chen, C. T. Liu, Z. P. Lu, *Adv. Mater.* **2010**, *22*, 2770.
[19] H. Guo, P. F. Yan, Y. B. Wang, J. Tan, Z. F. Zhang, M. L. Sui, E. Ma, *Nat. Mater.* **2007**, *6*, 735.
[20] Q. M. Peng, Y. D. Huang, L. Zhou, N. Hort, K. U. Kainer, *Biomaterials* **2010**, *31*, 398.
[21] J. Q. Wang, P. Yu, H. Y. Bai, *J. Non-Cryst. Solids* **2008**, *354*, 5440.
[22] *CRC Handbook of Chemistry and Physics* (Ed: D. R. Lide), 88th ed., Taylor & Francis Group, Boca Raton, FL **2008**.
[23] S. D. Soderquist, F. X. Kayser, *J. Less-Common Met.* **1968**, *16*, 361.
[24] J. Q. Wang, J. Y. Qin, X. N. Gu, Y. F. Zheng, H. Y. Bai, *J. Non-Cryst. Solids* **2011**, *357*, 1232.
[25] H. B. Yu, X. Shen, Z. Wang, L. Gu, W. H. Wang, H. Y. Bai, *Phys. Rev. Lett.* **2012**, *108*, 015504.
[26] J. J. Lewandowski, A. L. Greer, *Nat. Mater.* **2006**, *5*, 15.
[27] C. A. Schuh, A. C. Lund, T. G. Nieh, *Acta Mater.* **2004**, *52*, 5879.
[28] X. K. Xi, D. Q. Zhao, M. X. Pan, W. H. Wang, Y. Wu, J. J. Lewandowski, *Phys. Rev. Lett.* **2005**, *94*, 125510.
[29] D. V. Louzguine-Luzgin, A. R. Yavari, G. Q. Xie, S. Madge, S. Li, J. Saida, A. L. Greer, A. Inoue, *Phil. Mag. Lett.* **2010**, *90*, 139.
[30] J. H. Luo, F. F. Wu, J. Y. Huang, J. Q. Wang, S. X. Mao, *Phys. Rev. Lett.* **2010**, *104*, 215503.
[31] C. A. Volkert, A. Donohue, F. Spaepen, *J. Appl. Phys.* **2008**, *103*, 083539.
[32] P. Erne, M. Schier, T. J. Resink, *Cardiovasc Inter. Rad.* **2006**, *29*, 11.
[33] R. Waksman, R. Pakala, P. K. Kuchulakanti, R. Baffour, D. Hellinga, R. Seabron, F. O. Tio, E. Wittchow, S. Hartwig, C. Harder, R. Rohde, B. Heublein, A. Andreae, K. H. Waldmann, A. Haverich, *Catheter. Cardiovasc. Interv.* **2006**, *68*, 607.
[34] J. H. Nordlien, S. Ono, N. Masuko, K. Nisancioglu, *Corros. Sci.* **1997**, *39*, 1397.
[35] X. N. Gu, Y. F. Zheng, Y. Cheng, S. P. Zhong, T. F. Xi, *Biomaterials* **2009**, *30*, 484.
[36] Y. Shikinami, M. Okuno, *Biomaterials* **1999**, *20*, 859.
[37] J. Y. Suh, R. D. Conner, C. P. Kim, M. D. Demetriou, W. L. Johnson, *J. Mater. Res.* **2010**, *25*, 982.
[38] G. Wang, K. C. Chan, X. H. Xu, W. H. Wang, *Acta Mater.* **2008**, *56*, 5845.
[39] M. Q. Jiang, Z. Ling, J. X. Meng, L. H. Dai, *Philos. Mag.* **2008**, *88*, 407.
[40] X. X. Xia, W. H. Wang, *Small* **2012**, *8*, 1197.
[41] W. L. Johnson, K. Samwer, *Phys. Rev. Lett.* **2005**, *95*, 195501.
[42] J. Luo, H. P. Duan, C. L. Ma, S. J. Pang, T. Zhang, *Mater. Trans.* **2006**, *47*, 450.
[43] F. Zucchi, V. Grassi, A. Frignani, C. Monticelli, G. Trabanelli, *J. Appl. Electrochem.* **2006**, *36*, 195.
[44] T. Kokubo, H. Takadama, *Biomaterials* **2006**, *27*, 2907.